DOI: 10.1002/((please add manuscript number))
Article type: Communication

Atomic Layer Deposition of Rhenium Disulfide

Jani Hämäläinen, Miika Mattinen, Kenichiro Mizohata, Kristoffer Meinander, Marko Vehkamäki, Jyrki Räisänen, Mikko Ritala, and Markku Leskelä*

Dr. J. Hämäläinen, M. Mattinen, Dr. M. Vehkamäki, Prof. M Ritala, Prof. M. Leskelä
Department of Chemistry, University of Helsinki, P.O. Box 55, FI-00014 Helsinki, Finland
E-mail: jani.hamalainen@helsinki.fi
Dr. K. Mizohata, Dr. K. Meinander, Prof. J. Räisänen
Department of Physics, University of Helsinki, P.O. Box 64, FI-00014 Helsinki, Finland

Keywords: atomic layer deposition, ALD, rhenium sulfide, ReS_2, transition metal dichalcogenides

2D materials research is advancing rapidly as various new “beyond graphene” materials are fabricated, their properties studied, and materials tested in various applications. Rhenium disulfide is one of the 2D transition metal dichalcogenides (TMDCs) that has recently shown to possess extraordinary properties such as that it is not limited by the strict monolayer thickness requirements. The unique inherent decoupling of monolayers in ReS_2 combined with a direct bandgap and highly anisotropic properties make ReS_2 one of the most interesting 2D materials for a plethora of applications. In this paper, a highly controllable and precise atomic layer deposition (ALD) technique has been applied for the first time to deposit ReS_2 thin films. Film growth has been demonstrated on large area (5 cm × 5 cm) substrates at moderate deposition temperatures between 120 and 500 °C, and the films have been extensively characterized using FESEM/EDX, GIXRD, AFM, FIB/TEM, XPS, and TOF-ERDA techniques. The developed ReS_2 ALD process highlights the potential of the material for applications beyond planar structure architectures. The ALD process also offers a route to an upgrade to an industrial scale.

Since the isolation of monolayer graphene from bulk graphite and the discovery of its extraordinary properties in 2004,[1] the 2D materials research has been booming and a large array of "beyond graphene" materials have been introduced. Although 2D transition metal dichalcogenides were prepared already in 2005,[2] the discovery of a transition from indirect bandgap in bulk to direct bandgap in TMDC monolayers such as MoS_2 in 2010[3] ignited the 2D TMDC research towards various nanoelectronics and optoelectronics applications. This was further accelerated by development of wafer-scale synthesis of 2D TMDCs by chemical vapor deposition (CVD).[4]

Rhenium disulfide (ReS_2) is a unique material with surprising and attractive properties for the ever expanding 2D materials research. In 2014 it was shown[5] that in bulk ReS_2 the monolayers are effectively decoupled and thus the bulk remains a direct bandgap material regardless of the number of stacked monolayers. This is in total contrast to all the other semiconducting TMDCs, where direct bandgap is obtained only at a monolayer thickness. An extra valence electron (7 in total) in rhenium leads to a formation of additional Re–Re bonds and distorted octahedral (1T´) monolayer structure followed by effective decoupling of the monolayers in contrast to e.g. MoS_2 and WS_2.[5] The distorted 1T´ phase structure also has inherent reduced crystal symmetry, thus mono- and few-layer ReS_2 have been shown to have strongly in-plane anisotropic optical and transport properties.[6,7] As an example, anisotropic mobility ratio of 3.1 [b axis (120°)/a axis (0°)] has been reported, which was noted to be the highest experimentally determined value among all the known 2D materials.[8]

After the recent discovery of its unusual properties, ReS_2 has already been applied in field-effect transistors (FETs),[8,9,10,11,12,13,14,15,16,17,18] and several types of photodetectors.[9,15,19,20,21]

An integrated 2D digital inverter consisting of two ReS_2 anisotropic FETs,[8] as well as electric double-layer transistor with polymer electrolyte gating have been demonstrated.[22] As high as 79.1 cm^2/Vs field effect mobility was obtained for a 28 layer thick ReS_2 flake.[11] The photoresponsivity of 8.9×10^4 AW^{-1} reported by Liu et al.[21] in 2016 was claimed at the time to be the highest for any 2D material-based phototransistor with similar two-terminal structure. The high photoresponsivity resulted from increased light absorption originating from the thickness (2.5–4.5 nm) of a few ReS_2 layers. As followed, Shim et al.[18] showed a thicker (30 nm) ReS_2 photodetector to have a photoresponsivity as high as 2.5×10^7 AW^{-1} originating from both the high absorbance and direct bandgap properties of the ReS_2 film. In addition, ReS_2 has been suggested to be an excellent material for flexible electronic devices as the bandgap of ReS_2 monolayer has been calculated to be quite insensitive to strain (0.16 eV change from moving -2% compressive strain to 2% tensile strain).[23]

Use of ReS_2 in photocatalysis and catalysis has been discussed recently too.[24,25,26,27,28] Liu et al.[28] showed with *ab initio* calculations that ReS_2, both in monolayers and multilayers, should be stable and efficient photocatalyst for water splitting under visible light irradiation. ReS_2 on carbon foam was found to possess highly promising electrocatalytic properties for hydrogen evolution reaction (HER).[29] It has been speculated that perpendicular orientation of ReS_2 flakes to a substrate should be highly beneficial for HER due to an increased exposure of catalytically active edges of the crystal planes.[30] ReS_2 is also a candidate material for lithium-ion and lithium-sulfur batteries.[31,32] For further and more thorough survey of the current knowledge on 2D ReS_2, the recent review by Rahman et al.[33] is highly recommended.

Although mechanical exfoliation is a good method to study the suitability of 2D materials for various applications, for large scale production and industrial applications it is essential to

deposit 2D materials on large area substrates by vapor phase techniques.[34] It has been stated[34] that both CVD and atomic layer deposition (ALD) are nowadays the most widely used processes to prepare almost all kinds of electronic devices, and thus it would be highly desirable to deposit TMDCs with these methods for direct integration with the other materials. ALD,[35] a modification of CVD, is an unrivalled method for the deposition of thin films for the most advanced and demanding device structures. ALD is well known for its conformality and large area uniformity as well as simple and accurate film thickness and composition control combined with superior reproducibility and scalability. The saturative and self-limiting surface reactions provided by alternate precursor pulses result in these inherent advantages which are not as easily met with CVD. Therefore, development and characterization of ReS_2 ALD processes is of utmost importance and can lead to groundbreaking new applications.

Here, we introduce adoption of ALD for depositing ReS_2 for the first time. The films were grown using conventional and robust metal halide – H_2S based ALD chemistry at a wide deposition temperature range up to 500 °C on 5 cm × 5 cm substrate size. Conformal coating on a complex 3D test structure was also demonstrated. This work highlights that ALD as a highly controllable method, using simple and reliable metal halide-based chemistry, can be employed to grow the unorthodox 2D TMDC material ReS_2 which recently has been shown not to be restricted to a single, perfect monolayer thickness unlike all the other 2D materials. By controlling the film thickness and deposition temperature either smooth and well oriented films or edge exposing flakes standing up from the substrate plane can be obtained. This is important because various applications require different film morphologies.

Deposition temperature dependency of the ALD film growth was studied on in-situ Al_2O_3 coated Si(100) substrates (**Figure 1**). Successful film growth was obtained at a wide temperature range between 120 and 500 °C that was limited only by the source temperature needed to sublimate $ReCl_5$ (110 °C) and by the maximum temperature of the ALD reactor containing glass tubes (500 °C). The nominal growth rate increased from around 0.3 Å/cycle to close to 0.9 Å/cycle between 120 and 200 °C. At the same time the films changed from x-ray amorphous to crystalline (Figure 1c). The nominal growth rate was 0.8–0.9 Å/cycle at 200–300 °C and then steadily decreased to close to 0.2 Å/cycle at 450 °C. The decrease in the growth rate is linked to a decrease in the intensity of the wide peak around 32–34° and the appearance of the (001) orientation in the GIXRD patterns (Figure 1c). FESEM (Figure 1a) showed that up to 300 °C the ReS_2 crystals oriented parallel to the substrate while at 350 °C and above the platelike crystals were more randomly oriented with respect of the substrate. Because of this morphology, the thicknesses and growth rates measured by EDX need to be considered nominal at 350 °C and higher deposition temperatures. The nominal film thicknesses and growth rates were calculated assuming that the films are smooth, uniform and continuous, with a density of 7 g/cm^3 (bulk density of ReS_2 is 7.6 g/cm^3). All the crystalline films grown at 200 °C and above are ReS_2 according to the GIXRD patterns (Figure 1c) and the S/Re ratios determined by TOF-ERDA (Figure 1b). The surface roughnesses determined by AFM (Figure 1a, R_q) from the films with the randomly oriented ReS_2 crystals grown at 350 °C and above are close to the nominal film thicknesses obtained with EDX. In contrast, 80–90 nm thick ReS_2 films grown at 200–250 °C are very smooth having surface roughness of only about 2 nm, which increases to close to 6 nm for the film grown at 300 °C.

Detailed elemental compositions, impurity contents, and stoichiometry of the rhenium sulfide films grown at 120 and 500 °C were analyzed by TOF-ERDA and are represented in Table S1

and Table S2 (Supporting Information). The underlying Al_2O_3 film could not be distinguished reliably from ReS_2 and Si substrate by TOF-ERDA because of the upward orientation of the ReS_2 crystals and because of limited mass resolution separation of Al and Si was impossible. About 7 nm thick Al_2O_3 film was deducted from the results by assuming stoichiometric amounts of aluminum and oxygen in the Al_2O_3 films. According to the calculated S/Re ratios (1.8–2.1) the crystalline films grown at 200 °C and above seem to be stoichiometric ReS_2 (2.0) rather than Re_2S_7 (3.5). The amorphous films deposited at 150 °C and below contain large amounts of oxygen (18–28 at.%) suggesting that the films oxidized after the deposition or the growth was influenced by some volatile species of oxychlorides and oxides formed during the loading of the precursor as also noted in the TGA of $ReCl_5$ (Figure S1, Supporting Information). The oxygen content is around 3–4 at.% for the smooth, crystalline films and decreases to 1 at.% and less for the vertically standing ReS_2 crystals grown at higher temperatures. According to the XPS analyses (Table S3 and Table S4, Supporting Information) majority of the oxygen on the film surfaces is in hydroxyl groups, which suggests that the oxygen contamination (4–9 at.%) on the crystalline film surfaces originates from the exposure to the ambient after the deposition.

Growth rates of the films were investigated in more detail at 400 °C by varying both $ReCl_5$ and H_2S pulse lengths (**Figure 2**). At this temperature the films consist of the randomly oriented ReS_2 crystals. Saturation of the growth rates as typical for ALD was not achieved. Increasing the $ReCl_5$ pulse length was observed to decrease the nominal growth rate (Figure 2b) whereas increasing the H_2S pulse led to increased nominal growth rate (Figure 2d). Although reasons behind these observations are not clear, the non-saturative growth rates can be proposed to be due to the unique film morphology seen in the FESEM images (Figure 2a,c). The $ReCl_5$ and H_2S precursors have the opposite effect also on the film morphology.

Increasing $ReCl_5$ pulse length seems to lead to fewer vertically standing ReS_2 flakes (Figure 2a) whereas H_2S pulse increment results in areal densification of the flakes on the surface (Figure 2c).

Although no typical growth rate saturation was observed, the nominal film thickness increases linearly with increasing number of deposition cycles (**Figure 3**) as expected in an ALD process. The GIXRD patterns as a function of nominal film thickness (Figure 3c) reveal how the film growth progresses from x-ray amorphous to crystalline with visible (001) orientation after 200 deposition cycles, and additional orientations emerge in the films grown with ≥1500 cycles. Unfortunately, the anorthic ReS_2 has quite complicated XRD pattern with several orientations next to each other, thus specific peaks from the films could not be assigned with certainty.

The films grown at 300, 400, and 500 °C using 1000 cycles (Figure 1) were studied further by preparing cross-sectional TEM samples (Figure S2, Supporting Information). The film grown at 400 °C is also shown in **Figure 4**. The randomly oriented, crystalline ReS_2 film with a 32 nm nominal film thickness and surface roughness of 23 nm actually consists of about 10 nm thick uniform film oriented along the substrate and flakes of similar thickness emerging from the uniform film in directions away from the substrate plane. The ReS_2 monolayers are clearly identifiable from the TEM image. The interlayer spacing measured directly from the TEM image was 6.3 Å (Figure 4a). The corresponding interlayer spacings obtained from the films grown at 300, 400, and 500 °C (Figure S2, Supporting Information) were 6.5, 6.3, and 6.5 Å, respectively. The values are in good agreement with the reported interlayer spacing variance between 6.0 and 6.9 Å.[5] Furthermore, ReS_2 film growth was demonstrated on a 3D trench structure (Figure 4b), highlighting the benefits of ALD in depositing conformal film for

various applications on more demanding substrates than the commonly applied planar structures.

To summarize, ReS_2 growth has been realized by ALD using $ReCl_5$ and H_2S precursors at a wide deposition temperature range of 120 to 500 °C. Crystalline ReS_2 films with good quality were obtained at ≥200 °C. The film growth at 350 °C and above resulted in the randomly oriented flake like growth with identifiable stacked monolayer structures. The orientation parallel to the substrate, obtained at lower temperatures and small thicknesses, is attractive for microelectronics applications, whereas the vertical orientation is useful for those applications where high surface areas and edge exposure are important. Various starting surfaces, substrate pretreatments, addition of other precursors for doping and tuning the growth, and post-deposition treatments should be studied next to unleash the full potential of ALD ReS_2 for various applications. This could be beneficial for example for limiting the film growth only to conformal stacks of monolayers, for doping the material to tailor its properties, and etching the material to achieve more precise film morphology. Having a truly unique 2D material which is not limited by the number of stacked monolayers combined with a highly controllable ALD method that has already been widely adopted by the semiconductor industry could help to relieve restrictions in design architectures, adapt this material for new applications, and push forward industrial scalability of the 2D material applications.

Experimental Section

Rhenium sulfide thin films were deposited in a commercial F-120 ALD reactor (ASM Microchemistry Ltd., Finland) operated under reduced nitrogen pressure (AGA, 99.999 %, 10 mbar). The films were grown from rhenium pentachloride ($ReCl_5$, 99.9 %, Strem) and H_2S

(99.5 %, Linde) on in situ grown Al_2O_3 films. The Al_2O_3 ALD films (5–10 nm, 100 cycles) were deposited using $AlCl_3$ (99 %, Acros Organics) and deionized water (H_2O) on top of native oxide covered silicon (100) substrates (5 × 5 cm^2). The Si substrates were cut from 150 mm wafers supplied by Okmetic Oy (Finland). The solid $ReCl_5$ and $AlCl_3$ precursors were sublimed from open boats held inside the reactor at 110 and 80 °C, respectively, and pulsed with inert gas valving. $ReCl_5$ was loaded to the open boat in a glove box and transferred to the ALD reactor while covering the open boat with a sheet of flexible thermoplastic film (Parafilm M). H_2O was held in an external vessel at room temperature and pulsed into the reactor through needle and solenoid valves. H_2S flow rate (10 sccm) was set by a needle valve and a mass flow meter during continuous flow, and H_2S was pulsed into the reactor with a solenoid valve.

Thermogravimetric analysis (TGA) of $ReCl_5$ was done in a flowing nitrogen atmosphere (1 atm) by a Mettler Toledo Star^e system equipped with a TGA 850 thermobalance (Figure S1, Supporting Information). The $ReCl_5$ sublimation proceeded in three steps, where residues after each step were 13.2 %, 7.2 %, and a final residue of 1.6 %, respectively. The additional steps are most likely due to formation of other volatile species during a brief $ReCl_5$ air exposure before the measurement. These may comprise other chlorides, oxychlorides, and oxides. During the short air exposure while loading $ReCl_5$ into the ALD reactor, it formed visible fumes due to air exposure, and after depositions a dark residue was visible in the cold end of the source tube.

Crystallinity of the films was examined with a PANalytical X´Pert Pro x-ray diffractometer using grazing incidence (GIXRD) mode in angles between 10° and 65°. Surface morphology of the films was examined by a Hitachi S-4800 field emission scanning electron microscope

(FESEM). Nominal film thicknesses were determined using a GMRFilm electron probe thin film microanalysis program and energy-dispersive x-ray spectroscopy (EDX) data from an Oxford INCA 350 microanalysis system connected to the FESEM. It is emphasized that the nominal film thicknesses were calculated assuming that the films are smooth, uniform and continuous, with a density of 7 g/cm^3 (bulk density of ReS_2 is 7.6 g/cm^3).

Transmission electron microscopy (TEM) specimens were prepared with the focused ion beam (FIB) lift-out method, using a FEI Quanta 3D 200i DualBeam instrument. In the initial stage of the sample preparation, extra-long electron induced deposition steps of Pt-C composite were used to protect the extreme 2D surface shapes from ion damage. Bright-field TEM images were collected with a 200 kV Tecnai F20 transmission electron microscope.

Atomic force microscopy (AFM) images were recorded using a Veeco Multimode V instrument. Images were captured in tapping mode in air using silicon probes with a nominal tip radius of 10 nm and nominal spring constant of 40 N/m (RTESP from Bruker). Images were flattened to remove artefacts caused by sample tilt and scanner bow. Roughnesses were calculated as a root-mean-square values (R_q) from images (2×2 μm^2, 512×512 pixels) obtained at 0.5 Hz scan rate. Roughness calculations and flattening were done using a Bruker Nanoscope Analysis 1.5 program.

The composition of the surface layers was analyzed by x-ray photoelectron spectroscopy (XPS), using an Argus Spectrometer (Omicron NanoTechnology GmbH, Germany) operating at a pass energy of 20 eV. Samples were illuminated with x-rays emitted from a standard Mg source (K alpha line) at a photon energy of 1253.6 eV. Binding energies were calibrated using the C 1s peak (284.8 eV) of ambient hydrocarbons, and peak fitting was done using the

CasaXPS software. Re 4f energies were in good agreement with the values previously reported in the literature,[36] indicating that the samples predominantly contained Re(IV), within minor traces of Re at higher oxidation states, previously attributed to partially oxidised thin films.[37] Impurity contents of the films were determined with time-of-flight elastic recoil detection analysis (TOF-ERDA) by a 40 MeV $^{127}I^{10+}$ ion beam.

Supporting Information

Supporting Information is available from the Wiley Online Library or from the author.

Acknowledgements

The work was funded by the Finnish Center of Excellence in Atomic Layer Deposition (Academy of Finland).

Received: ((will be filled in by the editorial staff))
Revised: ((will be filled in by the editorial staff))
Published online: ((will be filled in by the editorial staff))

References

[1] K. S. Novoselov, A. K. Geim, S. V. Morozov, D. Jiang, Y. Zhang, S. V. Dubonos, I. V. Grigorieva, A. A. Firsov, *Science* **2004**, *306*, 666.

[2] K. S. Novoselov, D. Jiang, F. Schedin, T. J. Booth, V. V. Khotkevich, S. V. Morozov, A. K. Geim, *Proc. Natl. Acad. Sci. USA.* **2005**, *102*, 10451.

[3] K. F. Mak, C. Lee, J. Hone, J. Shan, T. F. Heinz, *Phys. Rev. Lett.* **2010**, *15*, 136805.

[4] Q. H. Wang, K. Kalantar-Zadeh, A. Kis, J. N. Coleman, M. S. Strano, *Nat. Nanotech.* **2012**, *7*, 699.

[5] S. Tongay, H. Sahin, C. Ko, A. Luce, W. Fan, K. Liu, J. Zhou, Y.-S. Huang, C.-H. Ho, J. Yan, D. F. Ogletree, S. Aloni, J. Ji, S. Li, J. Li, F. M. Peeters, J. Wu, *Nat. Commun.* **2014**, *5*, 3252.

[6] O. B. Aslan, D. A. Chenet, A. M. van der Zande, J. C. Hone, T. F. Heinz, *ACS Photonics* **2016**, *3*, 96.

[7] Y.-C. Lin, H.-P. Komsa, C.-H. Yeh, T. Björkman, Z.-Y. Liang, C.-H. Ho, Y. S. Huang, P.-W. Chiu, A. V. Krasheninnikov, K. Suenaga, *ACS Nano* **2015**, *9*, 11249.

[8] E. Liu, Y. Fu, Y. Wang, Y. Feng, H. Liu, X. Wan, W. Zhou, B. Wang, L. Shao, C.-H. Ho, Y.-S. Huang, Z. Cao, L. Wang, A. Li, J. Zeng, F. Song, X. Wang, Y. Shi, H. Yuan, H. Y. Hwang, Y. Cui, F. Miao, D. Xing, *Nat. Commun.* **2015**, *6*, 6991.

[9] F. Liu, S. Zheng, X. He, A. Chaturvedi, J. He, W. L. Chow, T. R. Mion, X. Wang, J. Zhou, Q. Fu, H. J. Fan, B. K. Tay, L. Song, R.-H. He, C. Kloc, P. M. Ajayan, Z. Liu, *Adv. Funct. Mater.* **2016**, 26, 1169.

[10] N. R. Pradhan, A. McCreary, D. Rhodes, Z. Lu, S. Feng, E. Manousakis, D. Smirnov, R. Namburu, M. Dubey, A. R. H. Walker, H. Terrones, M. Terrones, V. Dobrosavljevic, L. Balicas, *Nano Lett.* **2015**, *15*, 8577.

[11] B. Jariwala, D. Voiry, A. Jindal, B. A. Chalke, R. Bapat, A. Thamizhavel, M. Chhowalla, M. Deshmukh, A. Bhattacharya, *Chem. Mater.* **2016**, *28*, 3352.

[12] X. He, F. Liu, P. Hu, W. Fu, X. Wang, Q. Zeng, W. Zhao, Z. Liu, *Small* **2015**, *11*, 5423.

[13] K. Keyshar, Y. Gong, G. Ye, G. Brunetto, W. Zhou, D. P. Cole, K. Hackenberg, Y. He, L. Machado, M. Kabbani, A. H. C. Hart, B. Li, D. S. Galvao, A. George, R. Vajtai, C. S. Tiwary, P. M. Ajayan, *Adv. Mater.* **2015**, *27*, 4640.

[14] K. Xu, H.-X. Deng, Z. Wang, Y. Huang, F. Wang, S.-S. Li, J.-W. Luo, J. He, *Nanoscale* **2015**, *7*, 15757.

[15] E. Zhang, Y. Jin, X. Yuan, W. Wang, C. Zhang, L. Tang, S. Liu, P. Zhou, W. Hu, F. Xiu, *Adv. Funct. Mater.* **2015**, *25*, 4076.

[16] F. Cui, C. Wang, X. Li, G. Wang, K. Liu, Z. Yang, Q. Feng, X. Liang, Z. Zhang, S. Liu, Z. Lei, Z. Liu, H. Xu, J. Zhang, *Adv. Mater.* **2016**, *28*, 5019.

[17] C. M. Corbet, C. McLellan, A. Rai, S. S. Sonde, E. Tutuc, S. K. Banerjee, *ACS Nano* **2015**, *9*, 363.

[18] J. Shim, A. Oh, D.-H. Kang, S. Oh, S. K. Jang, J. Jeon, M. H. Jeon, M. Kim, C. Choi, J. Lee, S. Lee, G. Y. Yeom, Y. J. Song, J.-H. Park, *Adv. Mater.* **2016**, *28*, 6985.

[19] M. Najmzadeh, C. Ko, K. Wu, S. Tongay, J. Wu, *Appl. Phys. Express* **2016**, *9*, 055201.

[20] M. Hafeez, L. Gan, H. Li, Y. Ma, T. Zhai, *Adv. Funct. Mater.* **2016**, *26*, 4551.

[21] E. Liu, M. Long, J. Zeng, W. Luo, Y. Wang, Y. Pan, W. Zhou, B. Wang, W. Hu, Z. Ni, Y. You, X. Zhang, S. Qin, Y. Shi, K. Watanabe, T. Taniguchi, H. Yuan, H. Y. Hwang, Y. Cui, F. Miao, D. Xing, *Adv. Funct. Mater.* **2016**, *26*, 1938.

[22] D. Ovchinnikov, F. Gargiulo, A. Allain, D. J. Pasquier, D. Dumcenco, C.-H. Ho, O. V. Yazyev, A. Kis, *Nat. Commun.* **2016**, 7, 12391.

[23] Z. G. Yu, Y. Cai, Y.-W. Zhang, *Sci. Rep.* **2015**, *5*, 13783.

[24] T. Fujita, Y. Ito, Y. Tan, H. Yamaguchi, D. Hojo, A. Hirata, D. Voiry, M. Chhowalla, M. Chen, *Nanoscale* **2014**, *6*, 12458.

[25] K. Leiva, N. Martinez, C. Sepulveda, R. García, C. A. Jiménez, D. Laurenti, M. Vrinat, C. Geantet, J. L. G. Fierro, I. T. Ghampson, N. Escalona, *Appl. Catal. A* **2015**, *490*, 71.

[26] K. Leiva, C. Sepulveda, R. García, D. Laurenti, M. Vrinat, C. Geantet, N. Escalona, *Appl. Catal. A* **2015**, *505*, 302.

[27] Y. Huang, H. Liu, C. Ling, X. Chen, D. Zhou, S. Wang, *J. Phys. Chem. C* **2015**, *119*, 17092.

[28] H. Liu, B. Xu, J.-M. Liu, J. Yin, F. Miao, C.-G. Duan, X. G. Wan, *Phys. Chem. Chem. Phys.* **2016**, *18*, 14222.

[29] L. Wang, Z. Sofer, J. Luxa, D. Sedmidubský, A. Ambrosi, M. Pumera, *Electrochem. Commun.* **2016**, *63*, 39.

[30] J. Gao, L. Li, J. Tan, H. Sun, B. Li, J. C. Idrobo, C. V. Singh, T.-M. Lu, N. Korathar, *Nano Lett.* **2016**, *16*, 3780.

[31] Q. Zhang, S. Tan, R. G. Mendes, Z. Sun, Y. Chen, X. Kong, Y. Xue, M. H. Rümmeli, X. Wu, S. Chen, L. Fu, *Adv. Mater.* **2016**, *28*, 2616.

[32] J. Gao, L. Li, J. Tan, H. Sun, B. Li, J. C. Idrobo, C. V. Singh, T.-M. Lu, N. Korathar, *Nano Lett.* **2016**, *16*, 3780.

[33] M. Rahman, K. Davey, S.-Z. Qiao, *Adv. Funct. Mater.* **2017**, *27*, 1606129.

[34] M. Bosi, *RSC Adv.* **2015**, *5*, 75500.

[35] V. Miikkulainen, M. Leskelä, M. Ritala, R. L. Puurunen, *J. Appl. Phys.* **2013**, *113*, 021301.

[36] A. Naor, N. Eliaz, L. Burstein, E. Gileadi, *Electrochem. Solid-State Lett.* **2010**, *13*, D91.

[37] S. M. Davis, *Catal. Lett.* **1989**, *2*, 1.

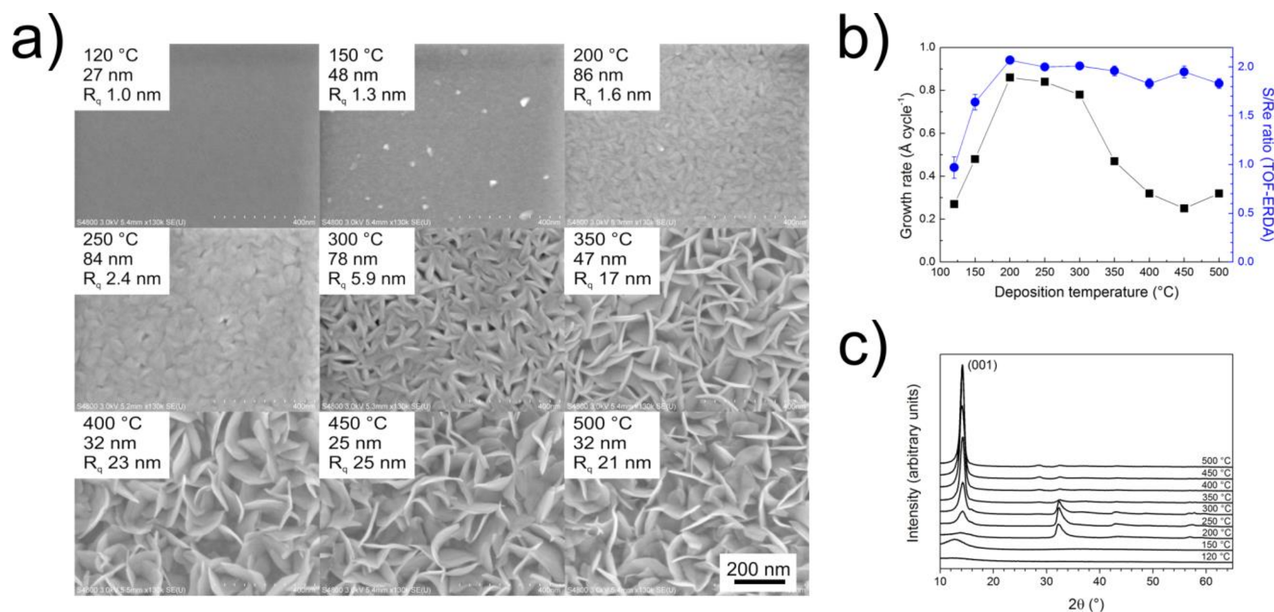

Figure 1. Rhenium sulfide films grown on Al_2O_3 films at various deposition temperatures. a) FESEM images with deposition temperatures, nominal film thicknesses (EDX), and surface roughnesses (R_q, AFM), b) nominal growth rate (EDX) and S/Re ratio (TOF-ERDA), c) GIXRD patterns. The pulse and purge lengths were 1 s each. The total number of deposition cycles was 1000.

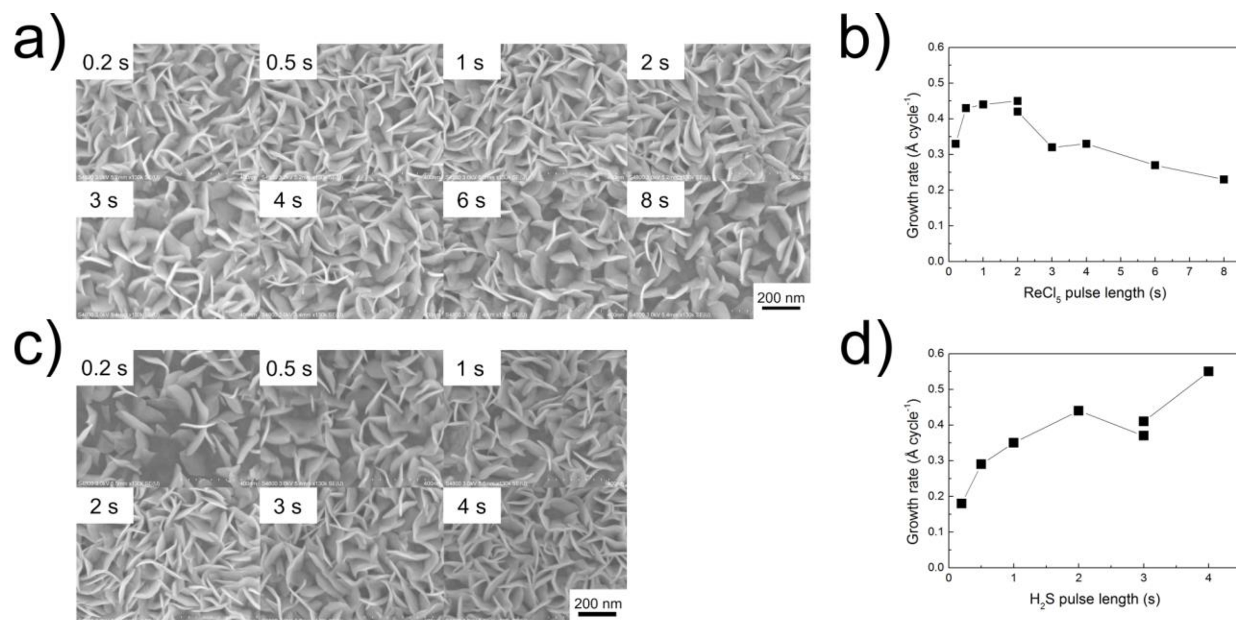

Figure 2. FESEM images and growth rate of the rhenium sulfide films grown on Al_2O_3 films at 400 °C as a function of both precursor pulses. a,b) $ReCl_5$ pulse, c,d) H_2S. The total number of deposition cycles was 1000. a,b) The pulse length of H_2S was 2 s, c,d) the pulse length of $ReCl_5$ was 1 s. All the purges were 1 s each.

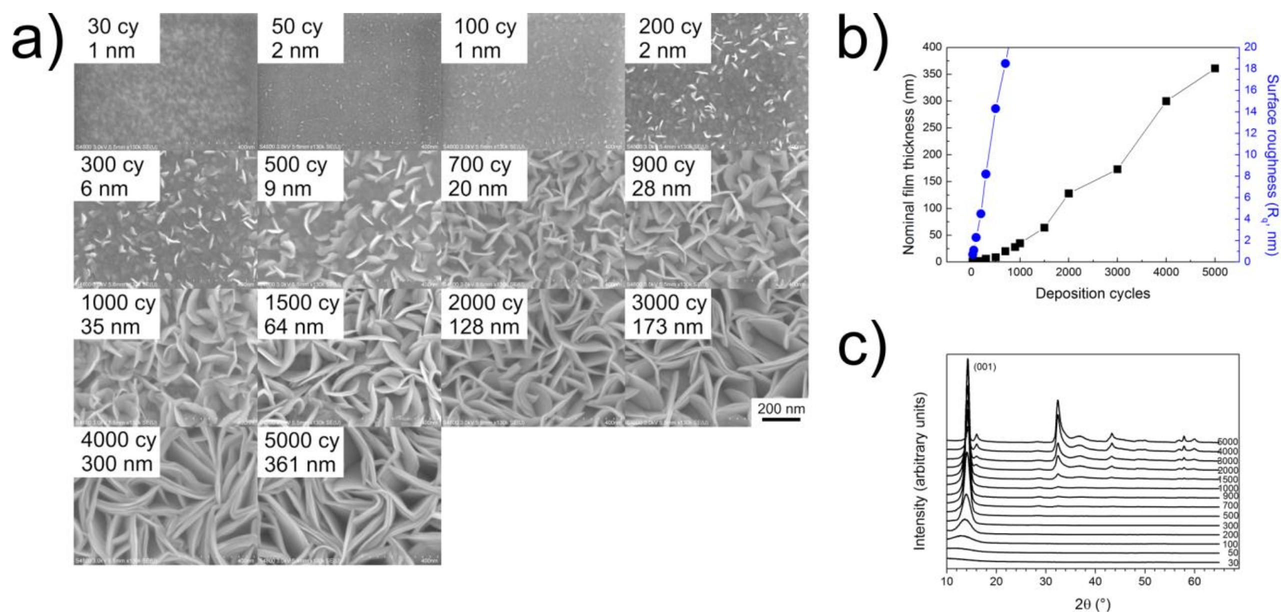

Figure 3. Rhenium sulfide films grown on Al_2O_3 films at 400 °C with varying number of deposition cycles. a) FESEM images with nominal film thicknesses, b) nominal film thicknesses (EDX) and surface roughnesses (AFM), c) GIXRD patterns. The pulse and purge lengths were 1 s each.

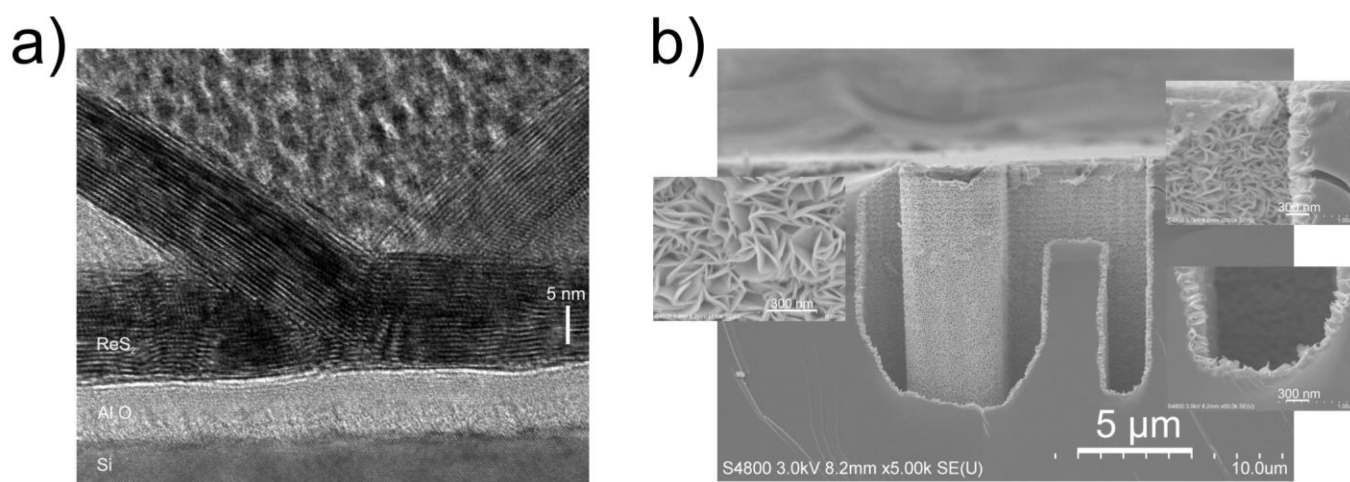

Figure 4. Rhenium sulfide films grown on Al_2O_3 films at 400 °C. a) cross-sectional TEM image of a film deposited using 1000 cycles. b) FESEM images of the film deposited on 3D structure using 2000 cycles.

Growth of rhenium disulfide by atomic layer deposition was studied. ReS_2 is a 2D material that is not limited to the monolayer thickness because of effective decoupling of the monolayers in bulk. The ReS_2 films were deposited from $ReCl_5$ and H_2S at up to 500 °C, also on a 3D structure, and the films were characterized.

atomic layer deposition, ALD, rhenium sulfide, ReS_2, transition metal dichalcogenides

J. Hämäläinen,* M. Mattinen, K. Mizohata, K. Meinander, M. Vehkamäki, J. Räisänen, M. Ritala, M. Leskelä

Atomic Layer Deposition of Rhenium Disulfide

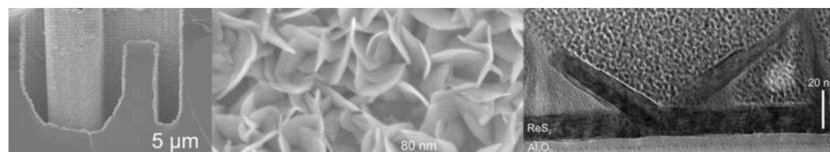

Copyright WILEY-VCH Verlag GmbH & Co. KGaA, 69469 Weinheim, Germany, 2016.

Supporting Information

Atomic Layer Deposition of Rhenium Disulfide

Jani Hämäläinen, Miika Mattinen, Kenichiro Mizohata, Kristoffer Meinander, Marko Vehkamäki, Jyrki Räisänen, Mikko Ritala, and Markku Leskelä*

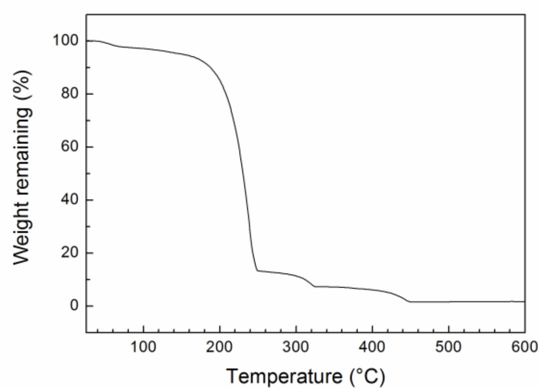

Figure S1. TGA curve measured for $ReCl_5$ under flowing N_2 atmosphere (1 atm).

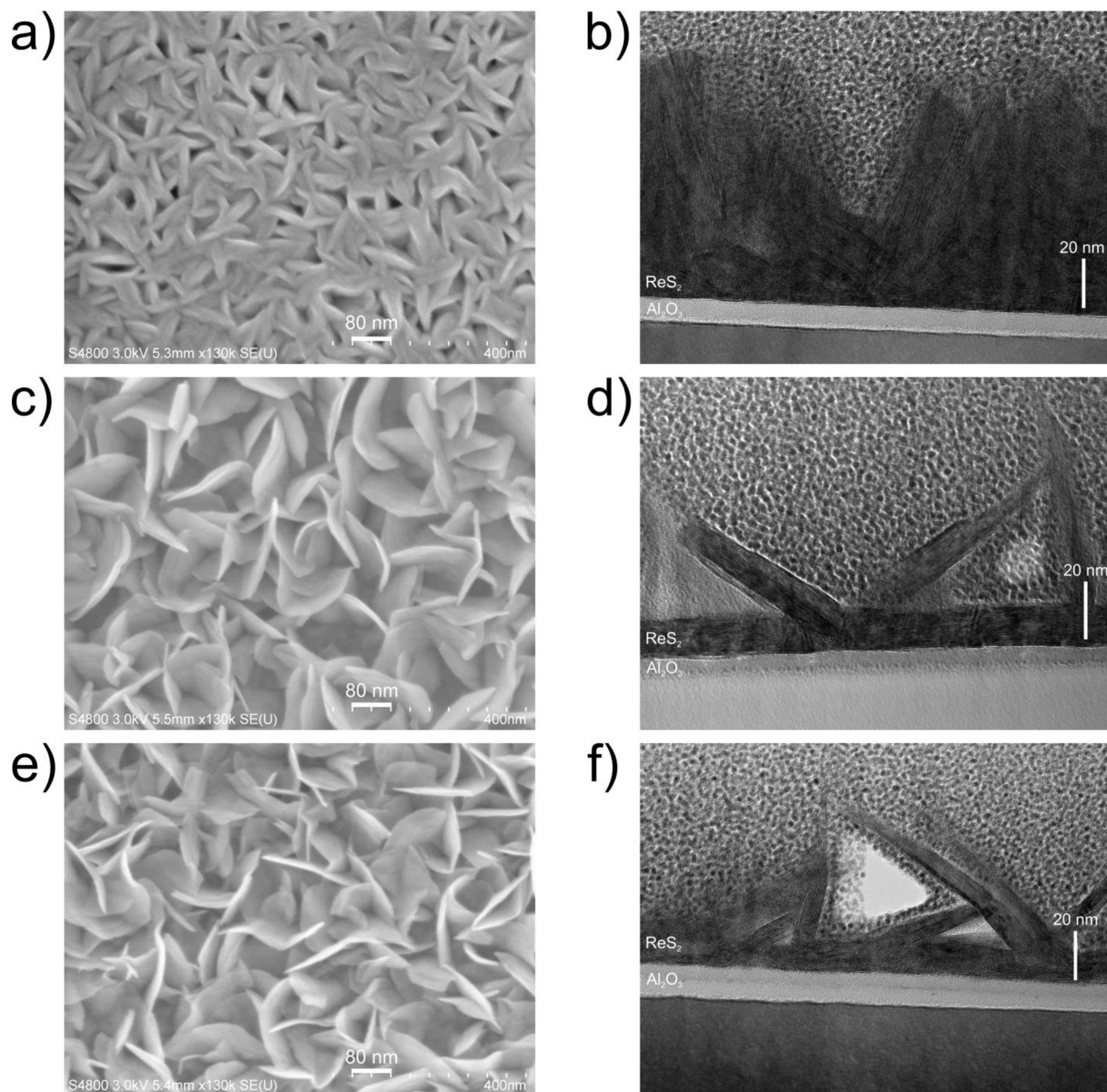

Figure S2. FESEM images and the corresponding cross-sectional TEM images of the films grown at a,b) 300, c,d) 400, and e,f) 500 °C.

Table S1. Elemental composition, impurity contents, and stoichiometry of the rhenium sulfide films deposited between 120 and 500 °C as analyzed by TOF-ERDA.

Dep. Temp.	120 °C	150 °C	200 °C	250 °C	300 °C	350 °C	400 °C	450 °C	500 °C
Re [at.%]	4.4 ± 0.3	12.5 ± 0.3	27.6 ± 0.2	29.3 ± 0.2	29.6 ± 0.3	28.2 ± 0.4	27.7 ± 0.4	27.6 ± 0.4	28.6 ± 0.4
S [at.%]	4.2 ± 0.5	20.5 ± 0.9	57.2 ± 0.8	58.6 ± 0.8	59.3 ± 0.9	55.1 ± 1.3	50.6 ± 1.2	53.8 ± 1.3	52.3 ± 1.3
Cl [at.%]	5 ± 2	10 ± 2	3.9 ± 0.3	2.08 ± 0.13	1.33 ± 0.08	0.06 ± 0.02	1.6 ± 0.2	0.05 ± 0.02	1.14 ± 0.12
H [at.%]	12 ± 4	9 ± 3	1.5 ± 0.4	0.6 ± 0.3	0.9 ± 0.3	1.8 ± 0.6	1.3 ± 0.4	2.2 ± 0.6	1.6 ± 0.5
C [at.%]	0.6 ± 0.3	0.5 ± 0.2	0.07 ± 0.02	0.08 ± 0.03	0.09 ± 0.03	0.38 ± 0.10	0.57 ± 0.12	0.63 ± 0.14	0.58 ± 0.12
O [at.%]	74 ± 3	48 ± 2	9.9 ± 0.4	9.4 ± 0.4	8.9 ± 0.4	14.6 ± 0.7	18.3 ± 0.8	15.7 ± 0.8	15.8 ± 0.8
S/Re ratio	0.97 ± 0.11	1.64 ± 0.08	2.07 ± 0.03	2.00 ± 0.03	2.01 ± 0.03	1.96 ± 0.05	1.83 ± 0.05	1.95 ± 0.06	1.83 ± 0.05

Table S2. Al_2O_3 underlayer corrected elemental composition, impurity contents, and stoichiometry of the rhenium sulfide films deposited between 120 and 500 °C as analyzed by TOF-ERDA.

Dep. Temp.	120 °C	150 °C	200 °C	250 °C	300 °C	350 °C	400 °C	450 °C	500 °C
Re [at.%]	12.0 ± 0.6	19.7 ± 0.5	29.5 ± 0.2	31.5 ± 0.3	32.0 ± 0.3	32.6 ± 0.4	33.9 ± 0.4	32.7 ± 0.4	34.0 ± 0.4
S [at.%]	11.7 ± 1.2	32.3 ± 1.4	61.1 ± 0.8	63.0 ± 0.9	64.2 ± 0.9	63.7 ± 1.4	61.8 ± 1.4	63.7 ± 1.5	62.1 ± 1.5
Cl [at.%]	12 ± 5	15 ± 3	4.2 ± 0.3	2.24 ± 0.14	1.44 ± 0.09	0.07 ± 0.02	2.0 ± 0.2	0.06 ± 0.02	1.35 ± 0.14
H [at.%]	34 ± 9	14 ± 4	1.6 ± 0.4	0.6 ± 0.3	0.9 ± 0.3	2.1 ± 0.7	1.5 ± 0.5	2.6 ± 0.7	1.9 ± 0.6
C [at.%]	1.7 ± 0.8	0.8 ± 0.3	0.07 ± 0.03	0.08 ± 0.03	0.10 ± 0.03	0.44 ± 0.12	0.69 ± 0.15	0.8 ± 0.2	0.69 ± 0.15
O [at.%][a)]	28.4 ± 1.1	17.6 ± 0.7	3.59 ± 0.13	2.65 ± 0.10	1.27 ± 0.05	1.11 ± 0.05	0.15 ± 0.01	0.21 ± 0.02	0.02 ± 0.02
S/Re ratio	0.97 ± 0.11	1.64 ± 0.08	2.07 ± 0.03	2.00 ± 0.03	2.01 ± 0.03	1.96 ± 0.05	1.83 ± 0.05	1.95 ± 0.06	1.83 ± 0.05

[a)] Equivalent amount of oxygen corresponding to about 7 nm Al_2O_3 underlayer has been substracted from the results.

Table S3. Surface analysis of elemental composition, impurity contents, and stoichiometry of the rhenium sulfide films deposited between 120 and 500 °C as analyzed by XPS.

Dep. Temp.	120 °C	150 °C	200 °C	250 °C	300 °C	350 °C	400 °C	450 °C	500 °C
Re [at.%]	15.4	16.0	20.1	21.3	21.0	24.0	21.9	25.0	25.3
S [at.%]	13.4	19.6	34.5	35.8	35.1	42.2	40.0	44.7	46.9
O [at.%]	17.2	11.1	9.2	8.6	7.0	5.3	7.2	4.6	3.7
C [at.%]	35.8	33.7	27.8	27.7	27.1	24.4	23.3	21.6	21.5
Cl [at.%]	12.7	16.4	4.8	2.8	6.4	1.0	0.4	0.2	0.1
Si [at.%]	5.5	3.1	3.6	3.9	3.5	3.2	7.3	4.0	2.4
S/Re ratio	0.9	1.2	1.7	1.7	1.7	1.8	1.8	1.8	1.9

Table S4. Relative contents of Re, Cl, and O oxidation states on the surface layers of the rhenium sulfide films deposited between 120 and 500 °C as analyzed by XPS.

Dep. Temp. [°C]	Re [%]				Cl [%]		O [%]		
	IV	V	VI	VII	Cl^-	organic-Cl	O^{2-}	OH^-	C=O
120	54.8	8.6	10.6	25.9	58.5	41.5	43.4	48.4	8.2
150	79.1	3.8	10.5	6.6	59.5	40.5	33.2	51.3	15.5
200	79.8	8.4	9.9	1.9	34.2	65.8	18.5	65.9	15.6
250	80.2	10.1	8.2	1.5	14.5	85.5	14.3	68.0	17.8
300	81.3	11.1	6.9	0.7	31.0	69.0	9.2	68.2	22.7
350	84.4	9.2	6.4	0.0	3.0	97.0	16.5	65.0	18.5
400	85.1	9.2	5.7	0.0	0.0	100.0	5.7	83.7	10.6
450	84.0	10.4	5.5	0.0	0.0	100.0	8.4	78.6	13.0
500	83.6	11.9	4.4	0.1	0.0	100.0	5.7	73.0	21.4